



Mechanical and Electrical Characterization of 8YSZ-ScCeSZ Ceramics

T. G. Fujimoto^{a*} V. Seriacopi^b L. A. S. Ferreira^a I. F. Machado^c E. N. S. Muccillo^a

^aInstituto de Pesquisas Energéticas e Nucleares (IPEN), Centro de Ciência e Tecnologia de Materiais (CCTM), 055508-000, São Paulo, SP, Brasil.

^bInstituto Mauá de Tecnologia (IMT), Departamento de Engenharia Mecânica, 09580-900, São Paulo, SP, Brasil.

^cUniversidade de São Paulo (USP), Escola Politécnica (Poli), 05508-030, São Paulo, SP, Brasil.

Received: December 16, 2022; Revised: March 23, 2023; Accepted: May 09, 2023

The effects of small amounts (up to 5 wt.%) of scandia- and ceria-stabilized zirconia on the electrical conductivity, and the elastic modulus and hardness of yttria-stabilized zirconia were investigated by impedance spectroscopy and nanoindentation tests, respectively. The main purpose of this work was to obtain solid electrolyte compounds with improved properties compared to those of the base materials. Solid electrolytes compounds were prepared by solid-state reaction synthesis with sintering at 1450 °C for 4 h. All prepared compounds exhibit a cubic fluorite-type structure. The microstructure of the compounds consists of polygonal grains with low (< 2%) porosity. The mean grain size estimated by the intercept method was 5 ± 1 µm. The electrical conductivity of the compound ceramics is lower than that of the base material. Addition of scandia-stabilized zirconia is found to exert a beneficial effect on the matrix by increasing the elastic modulus, achieving 221 MPa for 5 wt.% of the additive.

Keywords: *Yttria-stabilized zirconia, elastic modulus, electrical conductivity.*

1. Introduction

Over the last decades, the development of clean and sustainable energy sources has been one of the main subjects of scientific research. In this area, energy converters such as fuel cells, batteries and solar cells stand out, due to their promising contribution to reduce carbon emissions to the atmosphere¹.

Solid oxide fuel cells (SOFCs) are electrochemical devices for electric energy production with high efficiency, flexibility and low emission of pollutants². This type of device utilizes ceramic solid oxides like yttria-stabilized zirconia as solid electrolyte and operates at relatively high temperatures (800 - 1000 °C)^{2,3}. Nevertheless, at such high temperatures the rate of interfacial reactions among SOFC components increases and may influence its long-term performance. In addition, issues with the sealant, which must withstand several thermal cycles while maintaining its mechanical integrity, are prone to occur. To overcome those undesirable effects, most of the research work in recent years is concentrated in solid electrolytes able to operate in the so-called intermediate temperature (~550 to ~750°C) range with efficiency similar to the high-temperature SOFCs⁴⁻⁶. One approach to accomplish that goal is to exploit a mixture of solid electrolytes forming a compound or composite with improved properties compared to the individual materials. This strategy has long been used for other cell components⁷⁻¹⁰. In general, for application in SOFCs, the solid electrolyte must be as thin as possible to maximize its electrical performance and possess sufficient mechanical strength to support all sort of stresses imposed during fabrication and operation¹.

The electrical and mechanical properties of the composite solid electrolytes based on 8 mol% yttria-stabilized zirconia (8YSZ) and 3 mol% yttria stabilized zirconia (3YSZ) revealed increased fracture toughness accompanied by a slight improvement of the electrical conductivity¹¹. Nanocomposites of 8YSZ and yttria-doped ceria (YDC) with 1:1 volume ratio were investigated as a function of the particle size. Increase of the electrical conductivity and hardness was claimed, due to the size effect¹². 8YSZ was also added as a minor phase (up to 20 wt.%) to strontium- and magnesium-doped lanthanum gallate (LSGM). Reduction of the fraction of impurity phases, accompanied by a slight increase of the ionic conductivity were reported¹³. The addition of 8YSZ to Bi₂O₃ revealed a dual structure with high ionic conductivity and suitable thermal expansion coefficient up to 650 °C¹⁴. Recently, a LaNiO₃/YSZ composite electrolyte along with a Sr-free cathode was proposed to reduce the operation temperature of SOFCs¹⁵. Relatively few works are found in the reported literature on compound or composite electrolytes based on 8YSZ, particularly when this solid electrolyte is the major phase.

In this work, the influence of small amounts of zirconia-10 mol% scandia-1 mol% ceria, ScCeSZ, on the ionic conductivity and mechanical properties of 8YSZ was investigated by impedance spectroscopy and nanoindentation techniques.

2. Experimental

2.1. Sample preparation

Zirconia-8 mol% yttria (8YSZ, 99.6%, Tosoh, Japan) and zirconia-10 mol% scandia-1 mol% ceria (ScCeSZ, 99.98%,

*e-mail: talita.fujimoto@gmail.com

Fuel Cell Materials, USA) were used as starting materials without further purification.

Compound electrolytes of $(100-x)$ 8YSZ + x ScCeSZ, with $x = 0, 1$ and 5 wt.% (hereafter 8YSZ, 8YSZ-ScCeSZ1 and 8YSZ-ScCeSZ5, respectively) were synthesized by the solid-state reaction method. The starting materials were weighted in stoichiometric proportions after drying, mixed together in an agate mortar with isopropyl alcohol, and dried again in an oven. The powder mixture was pressed into pellets, (ϕ 9 mm and thickness of 3 mm) in a stainless steel dye, with 50 MPa applied pressure. Sintering of green pellets was carried out at 1450 °C for 4 h, in air, in a resistive furnace (Lindberg, BlueM) to generate dense specimens.

2.2. Characterization

The crystalline structure of sintered specimens was characterized by room-temperature X-ray diffraction, XRD, in a diffractometer (Bruker-AXS, D8 Advance), with 0.05° step size and 2 s counting time, and with Cu K_α ($\lambda = 1.5405$ Å) source, in the $20^\circ \leq 2\theta \leq 80^\circ$ range, with 40 kV and 30 mA. Identification of the crystalline phase was accomplished with PDF 30-1468 file of 8YSZ. The apparent density of pellets was determined by the immersion method with distilled water. The relative density, ρ_r , was calculated from Equation 1:

$$\rho_r = \left(\frac{\rho_m}{\rho_C} \right) \cdot 100 \quad (1)$$

where ρ_m and ρ_C are the measured and the compound electrolyte densities, respectively. The compound electrolyte density was obtained from Equation 2:

$$\rho_C = \rho_A V_A + \rho_B V_B \quad (2)$$

where ρ_i and V_i ($i = A, B$) are the crystallographic density and volume fraction, in weight percent, of 8YSZ and ScCeSZ, respectively.

Microstructure characterization was performed by field emission gun scanning electron microscopy, FEG-SEM (FEI, Inspect F50) for both powders and sintered pellets. Powders were spread out onto carbon tape, and sintered pellets were polished with diamond pastes (15, 6 and 1 μm), and thermally etched at 100 °C below the sintering temperature for this analysis. The mean grain size was estimated with ImageJ software.

Electrical conductivity measurements were carried out by impedance spectroscopy (Solartron, SI 1260) in the 10 Hz to 10 MHz and 500 to 800 °C frequency and temperature ranges, respectively. Impedance spectra were analyzed with ZView (Scriber Associates, Inc., USA) software utilizing the equivalent electric circuit model of Figure 1.

In this electric circuit model R1, CPE1 refers to the bulk and R2, CPE2 are due to interfaces. The R1 and R2 represent the electrical resistances and CPE1 and CPE2 symbolize the constant phase elements.

Nanoindentation tests were conducted with a triboindenter (Bruker, Hysitron TI 950) under maximum loads of 4 and 8 mN, with loading time of 5 s. Diamond indenter with Berkovich geometry was applied during tests. Load-displacement curves (P-h curves) were obtained for the samples. Reduced elastic modulus and indentation hardness can be predicted taking the data to be analyzed by Oliver-Pharr algorithm¹⁶.

In addition, the sample elastic modulus (E.M.) was calculated based on the reduced modulus (E_r) and indenter elastic modulus (E_i), and respective influences of Poisson ratios (v) according to Equation 3:

$$\frac{1}{E_r} = \frac{(1-v_i^2)}{E_i} + \frac{(1-v_s^2)}{E.M.} \quad (3)$$

3. Results and Discussion

Figure 2 shows scanning electron microscopy micrographs (secondary electron images) of the starting powders. 8YSZ (top) and ScCeSZ (bottom) powders consist of micrometer-sized spherical granules with large distribution in size, due to the production routes. Those granules are constituted by very small crystalline particles, similar to 25 nm for 8YSZ and lower than 100 nm for ScCeSZ.

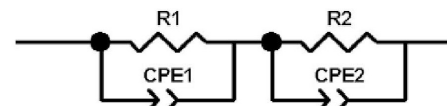


Figure 1. Equivalent electric circuit. R1 and R2 are resistances; CPE 1 and CPE2 are constant phase elements.

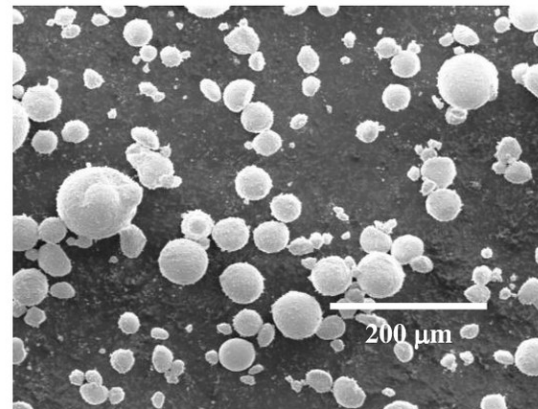
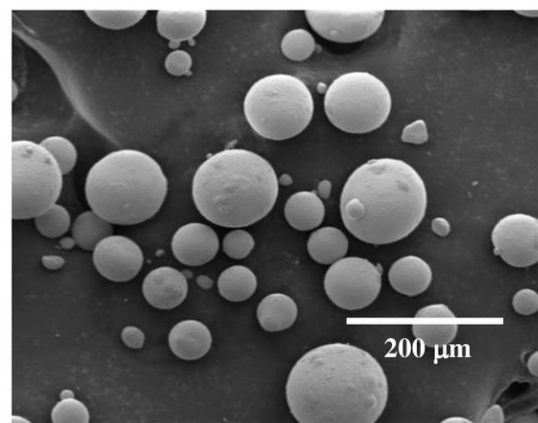


Figure 2. FEG-SEM micrographs of (a) 8YSZ and (b) ScCeSZ starting powders.

The starting powders form soft agglomerates after mixing together, which are broken or disintegrated during conformation, leading to high density specimens after sintering at 1450 °C for 4 h. The relative density of all sintered pellets is high, similar to 97% of the theoretical value. There is a tendency to decrease the density, 97.9% (8YSZ), 97.7% (1 wt.%) and 97.1% (5 wt.%) of compounds with increasing the amount of ScCeSZ. The apparent porosity is also low, less than 2% for all sintered pellets.

The XRD patterns of sintered compounds are depicted in Figure 3. The 8YSZ specimen displays the characteristic cubic fluorite-type crystalline structure (*Fm3m* space group) according to PDF 30-1468. Other compound electrolytes reveal equivalent XRD profile. This result was expected, because ScCeSZ also has the cubic structure for sintering temperatures above 1300 °C¹⁷. No impurity phases were detected.

The sintered pellets exhibit similar microstructure features. Figure 4 shows, as an example, typical FEG-SEM micrographs of (a) 8YSZ and (b) 8YSZ-ScCeSZ5. The microstructure of sintered pellets consists of polygonal grains. The average grain size of sintered specimens, about $5 \pm 1 \mu\text{m}$, is relatively large. Randomly distributed pores are found at grain boundaries and inside the grains. No undesirable features like abnormal grain growth, cracks and segregated phases were found. Other compound electrolytes display alike microstructure.

Figure 5 shows impedance spectroscopy spectra of 8YSZ (top) and 8YSZ-ScCeSZ5 (bottom) recorded at 525 and 500 °C, respectively. These diagrams consist of a large arc due to capacitive and resistive effects of the bulk. The arc attributed to grain boundaries/interfaces usually detected between those of the bulk and of the electrodes, is known to become negligible in polycrystalline ceramics with grain sizes higher than $5 \mu\text{m}$ ¹⁸. Nevertheless, in the frequency range around 100 kHz, the impedance diagram of the pellet containing ScCeSZ is flattened reflecting some differences in the grain boundary/interface region. This difference may be a consequence of a composite formation between 8YSZ and ScCeSZ, although some solubility may be expected. The impedance spectroscopy response of the specimen containing 1 wt.% ScCeSZ is quite similar to that of the base ceramic 8YSZ.

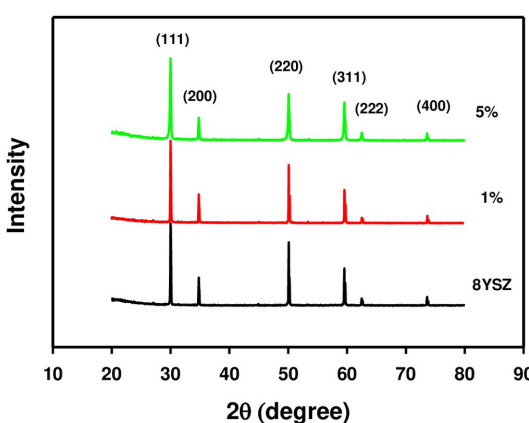


Figure 3. XRD patterns of sintered pellets: 8YSZ, 8YSZ-ScCeSZ1 (1%) and 8YSZ-ScCeSZ5 (5%).

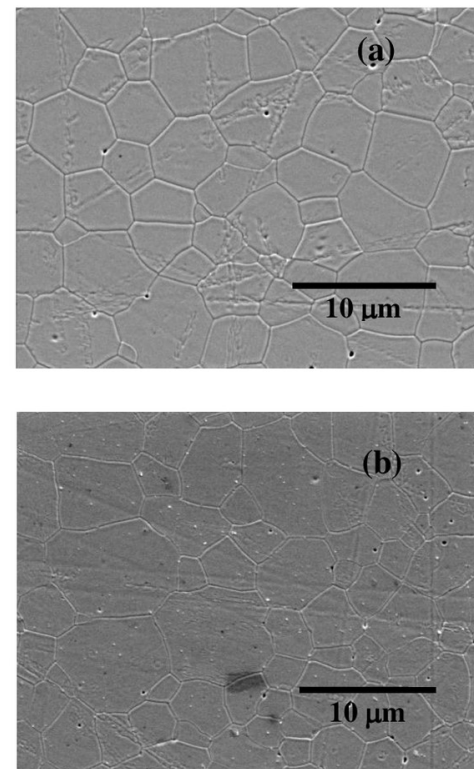


Figure 4. FEG-SEM micrographs of (a) 8YSZ and (b) 8YSZ-ScCeSZ5 pellets sintered at 1450 °C/4 h.

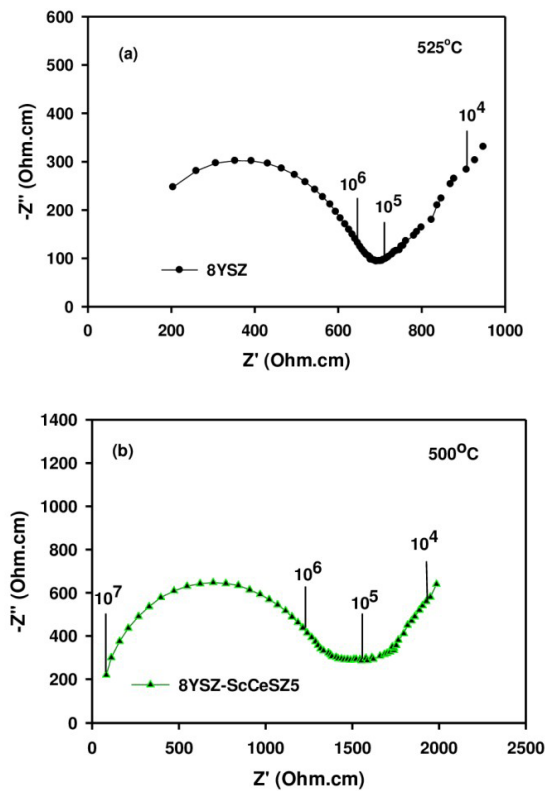
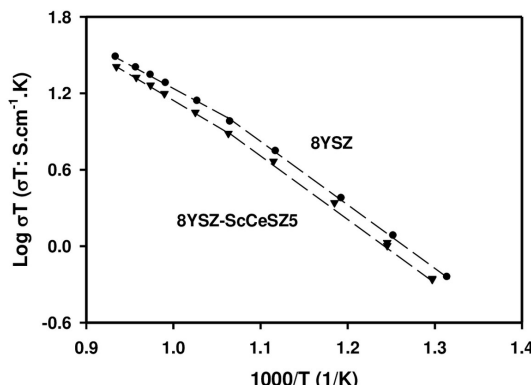
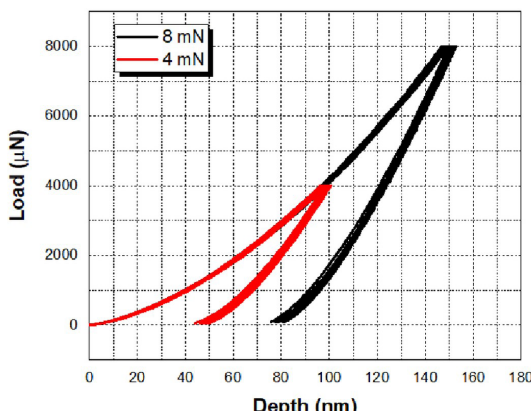


Figure 5. Impedance spectroscopy diagrams of 8YSZ (top) and 8YSZ-ScCeSZ5 (bottom) specimens.

Table 1. Values of hardness and elastic modulus (E.M.) of sintered specimens.

Specimen	Load (mN)	Hardness (GPa)	E.M. (GPa)	Load (mN)	Hardness (GPa)	E.M. (GPa)
8YSZ	4	19.0±0.5	211.7±3.4	8	18.2±0.3	205.8±5.3
1 wt.% ScCeSZ	4	18.0±0.7	216.5±7.1	8	17.4±0.7	216.4±4.4
5 wt.% ScCeSZ	4	18.2±0.4	221.0±4.0	8	18.2±0.4	216.7±5.2

**Figure 6.** Arrhenius plots of the electrical conductivity of 8YSZ and 8YSZ-ScCeSZ5.**Figure 7.** Load-displacement (P-h) curves of 8YSZ for 4 and 8 mN.

Analysis of the impedance spectroscopy diagrams in the whole temperature range of measurements allowed for obtaining the Arrhenius plots of the bulk conductivity shown in Figure 6. Addition of ScCeSZ to 8YSZ resulted in a small decrease in the electrical conductivity. This unexpected result may be a consequence of some kind of interaction between both electrolytes during sintering. Straight lines were obtained in the temperature range of measurements for all compounds, with a change of slope at approximately 650 °C. In the low-temperature range the activation energies were 0.96±0.05 (8YSZ) and 0.98±0.05 eV (8YSZ-ScCeSZ5). The activation energy for conduction decreases to 0.73±0.5 (8YSZ) and 0.79±0.05 eV (8YSZ-ScCeSZ5) in the high-temperature range. This difference in the activation energy, in the low- and high-temperature ranges, (about 0.2 eV) is usually assigned to complex defects formed at low temperatures¹⁹.

Nanoindentation tests were performed on sintered pellets. Figure 7 shows, as example, typical load-displacement (P-h) curves of 8YSZ for 4 and 8 mN loads. The obtained hardness and elastic modulus are summarized in Table 1 for all sintered pellets.

The hardness values obtained for 8YSZ are in the 18–19 GPa range, in agreement with previous work²⁰. Addition of ScCeSZ to 8YSZ exerts a minor influence on the hardness of the compound materials. In contrast, the elastic modulus increases with increasing the amount of ScCeSZ (Table 1).

4. Conclusions

Compound electrolytes constituted by mixtures of yttria-stabilized zirconia and scandia- and ceria-doped zirconia were successfully prepared by solid-state reaction. The crystalline structure and the microstructure of sintered compounds are similar to that of 8YSZ. The relative density of the compounds is high (~97% of the theoretical value) and the porosity is negligible (<2%). The estimated mean grain size is 5±1 μm. The electrical conductivity of 8YSZ decreases with addition of ScCeSZ. Results from nanoindentation experiments reveal that the hardness remains approximately constant. In contrast, the elastic modulus tends to increase with increasing amounts of ScCeSZ. The dispersion measurements (standard deviation) can be assigned to the local and microstructural effects.

5. Acknowledgements

The authors acknowledge FAPESP (2013/07692-2), CNPq (305889/2018-4), CAPES (Finance code 0001) and CNEN for financial supports.

6. References

1. Stambouli AB, Traversa E. Solid oxide fuel cells (SOFCs): a review of an environmentally clean and efficient source of energy. *Renew Sustain Energy Rev.* 2002;6:433-55.
2. van Gool W, Hagenmuller P. Solid electrolytes: general principles, characterization, materials, application. New York: Academic Press; 1978.
3. Subbarao EC. Solid electrolytes and their applications. New York: Plenum; 1980.
4. Ralph JM, Schoeler AC, Krumpelt M. Materials for lower temperature solid oxide fuel cells. *J Mater Sci.* 2001;36:1161-72.
5. Doshi R, Richards VL, Carter JD, Wang X, Krumpelt M. Development of solid-oxide fuel cells that operate at 500 °C. *J Electrochem Soc.* 1999;14:1273-8.
6. Gao Z, Mogni LV, Miller EC, Railsback JG, Barnett SA. A perspective on low-temperature solid oxide fuel cells. *Energy Environ Sci.* 2016;9:1602-44.
7. Baek SK, Jeong J, Schlegl H, Azad AK, Park DS, Baek UB, et al. Metal-supported SOFC with an aerosol deposited in-situ LSM and 8YSZ composite cathode. *Ceram Int.* 2016;42:2402-9.

8. Farhan S, Mohsin M, Raza AH, Anwar R, Ahmad B, Raza R. Co-doped cerium oxide $\text{Fe}_{0.25x}\text{Mn}\text{Ce}_{0.75}\text{O}_{2-\delta}$ as composite cathode material for IT-SOFC. *J Alloys Compd.* 2022;906:164319.
9. Fonseca FC, de Florio DZ, Esposito V, Traversa E, Muccillo ENS, Muccillo R. Mixed ionic-electronic YSZ/Ni composite for SOFC anodes with high electrical conductivity. *J Electrochem Soc.* 2006;153:A354-60.
10. Guesnet L, Aubert G, Hubert S, Geffroy PM, Aymonier C, Bassat JM. Infiltration of nickel and copper catalysts into a GDC backbone assisted by supercritical CO_2 for efficient SOFC anodes. *Sustain Energy Fuels.* 2022;6:1801-11.
11. Fernandes CM, Castela A, Figueiredo FM, Frade JR. Microstructure-property relations in composite yttria-substituted zirconia solid electrolytes. *Solid State Ion.* 2011;193:52-9.
12. Bellino MG, Lamas DG, Reca NEW. Preparation and ionic transport properties of YDC-YSZ nanocomposites. *J Mater Chem.* 2008;38:4537-42.
13. Fujimoto TG, Reis SL, Muccillo ENS. Influence of yttria-stabilized zirconia on microstructure and electrical properties of doped lanthanum gallate. *Mater Res.* 2019;22:e20190043.
14. Liu LF, Cheng YH, Wei WCJ. Processing of high conductivity Bi_2O_3 /8YSZ composites as SOFC electrolyte. *J Ceram Process Res.* 2019;20:347-56.
15. Nie JJ, Zheng D, Ganesh KS, Akbar M, Xia C, Dong WJ, et al. Efficient strategy to boost the electrochemical performance of yttrium-stabilized zirconia electrolyte solid oxide fuel cell for low-temperature applications. *Ceram Int.* 2021;47:3462-72.
16. Oliver WC, Phar GM. Measurement of hardness and elastic modulus by instrument indentation: advances in understanding and refinements of methodology. *J Mater Res.* 2004;19:3-20.
17. Gross RL, Muccillo ENS. Sintering, phase composition and ionic conductivity of zirconia-scandia-ceria. *J Power Sources.* 2013;233:6-13.
18. Kleitz M, Bernard H, Fernandez E, Schouler E. Impedance spectroscopy and electrical resistance measurements on stabilized zirconia. In: Heuer AH, Hobbs LW, editors. *Science and Technology of Zirconia I.* Cleveland: The American Ceramic Society; 1981. p. 310-336.
19. Zhang L, Virkar AV. On space charge and spacial distribution of defects in yttria-stabilized zirconia. *J Electrochem Soc.* 2017;164:F1506-23.
20. Lian J, Garay JEJ, Wang J. Grain size and grain boundary effects on the mechanical behavior of fully stabilized zirconia investigated by nanoindentation. *Scr Mater.* 2007;56:1095-8.